Dynamical Arrest in Superionic Crystals and Supercooled Liquids†

Angus Gray-Weale* and Paul A. Madden

Physical and Theoretical Chemistry Laboratory, University of Oxford, South Parks Road, OX1 3QZ, U.K.

Received: December 4, 2003; In Final Form: March 19, 2004

Phenomenological similarities between the temperature dependence of the thermal and transport properties of supercooled liquids and certain crystalline fast-ion conductors are explored, using information from computer simulations and experiments. The similarities include non-Arrhenius temperature dependence of the transport coefficients, anomalies in the heat capacity, two-step relaxation of the time-correlation functions, and the connection between the mobility and entropy being described by the Adam−Gibbs equation. We use the detailed information available from computer simulation to examine the relationship between these observations and the number of defects in the system. Such defects may be unambiguously identified in a simple geometrical way from the underlying lattice in the superionic system; defects are often invoked in descriptions of supercooled liquid behavior but they are not easily defined in such a strongly disordered system.

1. Introduction

Many fluorite-structured ionic materials exhibit a continuous transition to a highly conducting state, in which the mobility of one species reaches liquid-like values. The transition is accompanied by a decrease in density and a heat-capacity peak, but no change in the average crystal structure (a type-II superionic transition).[1] Examples include lead fluoride and calcium fluoride, where the fluoride ion is the mobile species, and the anti-fluorite lithium oxide, in which the cation is mobile. It has been appreciated for some time that the strong temperature dependence of the thermal and transport properties close to the superionic transition cannot be explained by the thermal excitation of a number of independently mobile point defects. There is a strong element of "cooperativity". Diffraction studies show a high proportion of the mobile species move off their lattice sites during the transition, and the diffuse scattering shows that the resulting defects have a considerable degree of spatial correlation.[2,3] These observations have been replicated in computer simulations, such as the ones we discuss below.[4,5]

There have been numerous models for the origin of the cooperativity via an explanation of this rapid increase in the number of defects. In particular, a finite concentration of defects could affect the free energy needed to excite another by changing the screening properties of the lattice or by changing its elastic properties, which would influence the Coulombic interactions or strain energy. However, the experimental data do not differentiate between the predictions of these models, which lead to very similar expressions when reduced to a tractable form, and it seems desirable to first approach the cooperativity from as general a perspective as possible, without initially identifying key interactions at a microscopic level. We note some common features with the emerging understanding of the glass transition, where there is an intense dialogue involving analyses derived from microscopically based models and more general formulations, such as the energy-landscape picture or mode-coupling theory. The purpose of this paper is to point out some similarities between the phenomena exhibited at the transitions, with the objective of motivating a subsequent analysis of the superionic behavior with the ideas used to describe the glass transition.

Although our purpose is to indicate similarities, we should emphasize some key differences. First, the superionic systems are in thermal equilibrium, whereas a key aspect of the glass is that it is "ill-condensed" and not ergodic. By drawing the analogy at the phenomenological level we may therefore help to focus attention on those aspects of the glass transition that are truly related to its out-of-equilibrium character. Second, at all temperatures the structures of the ionic conductors are based upon a well-defined crystalline lattice. This means that the concept of a "defect" has a well-defined geometrical basis. Numerous models of glassy behavior are based upon the idea of defects as representative excitations of ill-defined ideal amorphous networks.[6,7] It may be that such models could be applied quantitatively to the superionic systems, whereas their applicability to glasses rests very heavily on this initial conjecture.

Section 2 describes the details of the potentials and methods used in the present computer simulations. In section 3 we draw attention to the phenomenological similarities between glass formers and superionics, and then in section 4 we discuss how these phenomena in the superionic might be related to the formation and interaction of mobile defects. Section 5 examines some simple, mean-field models for the defects and the thermodynamic properties. Our conclusions are given in section 6.

2. Simulation Studies

We concentrate on two materials, calcium fluoride and lead-(II) fluoride, in which the fluoride ions are mobile. These systems are representative of the range of behavior exhibited by fluorite-structured systems with type-II transitions.[8,9] PbF_2 shows a sharp transition, with a rapid increase in the conductivity with temperature and a pronounced heat capacity peak, whereas the increase is more gradual in CaF_2 and the peak in the heat capacity much lower. Because of the comparative low transition temperature in PbF_2 (∼700 K, compared to ∼1450 K for CaF_2)

† Part of the special issue "Hans C. Andersen Festschrift".

* Corresponding author.

10.1021/jp037706a CCC: $27.50
Published on Web 05/05/2004

TABLE 1: Temperature, Scaled Temperature, Unit Cell Length (a), and Number Density (ρ) of Ions Used in the MD Simulations of Calcium Fluoride[a]

T(K)	T/T_c	a(Å)	ρ(Å^{-3})
1100	0.759	5.565	0.0696
1200	0.828	5.578	0.0691
1350	0.931	5.160	0.0680
1400	0.966	5.617	0.0677
1450	1.000	5.627	0.0674
1500	1.035	5.636	0.0670
1550	1.069	5.644	0.0667
1600	1.103	5.653	0.0664
1650	1.138	5.662	0.0661
1700	1.172	5.667	0.0659
1800	1.241	5.682	0.0653
1900	1.310	5.698	0.0649

[a] The timestep was 20.0 au $= 4.82 \times 10^{-5}$ ps. Two sets of runs were performed: some of 10^5 steps and some with nearly 10^6 steps. The shorter runs were sufficient for many quantities. The longer runs were necessary for self-intermediate scattering function, for instance. Details of the potential may be found in reference 10.

TABLE 2: Temperature, Scaled Temperature, Unit Cell Length, and Number Density of Ions Used in the MD Simulations of Lead Fluoride[a]

T(K)	T/T_c	a(Å)	ρ(Å^{-3})
300	0.3205	5.939	0.0573
700	0.7479	6.016	0.0551
800	0.8547	6.039	0.0545
850	0.9081	6.054	0.0541
900	0.9615	6.069	0.0537
925	0.9882	6.086	0.0532
950	1.0150	6.118	0.0524
975	1.0417	6.146	0.0517
1000	1.0684	6.195	0.0515
1100	1.1752	6.195	0.0505
1200	1.2821	6.255	0.0490

[a] The timestep and run lengths are as described in Table 1 for calcium fluoride. Details of the potential may be found in references 4 and 5.

it has been the subject of more detailed experimental studies of the structure and dynamics.

The potential used for lead fluoride permits dipolar polarization of both species, which gives it a many-body character, and the Car−Parrinello method is used to solve for the dipoles "on-the-fly". The short-range parts of the potential were derived from ab initio electronic structure calculations: more details of the simulation of lead fluoride are given in references 4 and 5. The potential reproduces the properties of PbF_2 well, though the transition temperature is too high at ~940 K,[5] compared to the real material at 702 K.[2] For CaF_2, where the cation is much less polarizable than in PbF_2, we used a simpler pair potential extensively studied by Gillan.[10] In previous work,[11] we have compared the properties predicted by this empirical pair potential with those predicted by an ab initio polarizable potential, analogous to that used for PbF_2, and found almost no difference in the superionic phase (though there are differences at melting). We have therefore used the pair potential because of the lower computational cost.

We calculated molecular dynamics trajectories at a series of temperatures covering the superionic transitions, using the usual methods, such as periodic boundary conditions and an Ewald sum for the long-ranged forces.[12] The density for each temperature (listed in Tables 1 and 2) was chosen from an initial constant-pressure molecular dynamics run at zero pressure. Constant-volume runs were then used to collect the data reported below, except for the isobaric heat capacities which come from constant-pressure runs. These ensembles were implemented with the thermostat and barostat described in references 13 and 14. The thermostat and barostat relaxation times were long enough that they do not interfere with the dynamical processes of interest. The time step in all simulations was 20.0 au $= 4.82 \times 10^{-4}$ ps. The calcium fluoride results are taken from runs of 10^5 steps with 1500 ions, except for the time correlation functions, which come from 324 ion runs of nearly 10^6 steps. All lead fluoride calculations had 324 ions, and again 10^5 steps were enough for most properties, but nearly 10^6 steps were necessary for the time correlation functions.

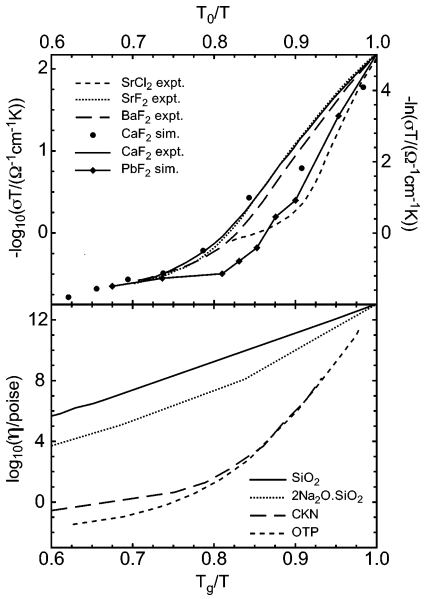

Figure 1. Viscosities of four glass formers (bottom) and the conductivities of several fluorite-structured superionics (top), against scaled temperature. Note that the conductivities decrease up the page, i.e., we have plotted resistivities. The profiles are similar. The temperature is scaled for the glass formers by the experimental glass transition, and for the superionics as discussed in the text. The position of T_0 makes little difference to the appearance of this plot. Varying degrees of curvature appear in both plots. Note though that the glass formers' viscosities vary over many more orders of magnitude. The experimental conductivity data are digitized from reference 8, and the viscosity data from reference 15.

3. Similarities between Superionics and Glass Formers

3.1. Mobilities. The loss of fluidity of a supercooled liquid close to its glass transition is characterized by an increase in the viscosity and often represented on an "Angell plot",[15] in which the logarithm of the viscosity is plotted against the inverse of a temperature, which is scaled by its value where the viscosity reaches 10^{13} poise, the experimental glass transition. Such a plot is shown in the bottom half of Figure 1.[15] Supercooled liquids may be classified as strong or fragile using the Angell plot. Strong glass formers have Arrhenius viscosities (a linear Angell plot), as if some simply activated process were responsible for the relaxation of shear stresses. Strong liquids are often ionic network-formers, like SiO_2 or $2Na_2O{\cdot}SiO_2$. In a fragile glass former, the viscosity increases slowly with decreasing temperature through the normal liquid range and on weak supercooling, but then increases rapidly toward the glass transition. Such behavior is often represented empirically by a Vogel−Fulcher−Tamman expression. The fragile liquids tend to be unassociated (like calcium potassium nitrate, CKN, or o-terphenyl, OTP) and the loss of fluidity occurs because of the slowing of cage relaxation. This is regarded as a cooperative

process involving the reorganization of progressively more particles with increasing energy cost as the temperature is lowered.

The ionic conductivity is the appropriate, readily observable measure of mobility in superionics. In the upper half of Figure 1, we show the resistivities, or inverse conductivities, from our simulations[5] and recently published experiments,[8] in order to make the analogy with the viscosity. These too are plotted against the inverse of a scaled temperature in the manner suggested by the Angell plot of viscosity. The superionics' conductivities have various curvatures as the transition is approached from above, like the viscosities of glass-forming liquids. The simplest model of ion conduction in a crystal envisages the thermal excitation of Frenkel defects (a vacancy-interstitial pair) which then hop through the lattice. One would expect this process to give rise to a simple Arrhenius behavior for the conductivity, with the Arrhenius energy reflecting the formation and migration energy of the defects.[1] The non-Arrhenius temperature dependence can be regarded as a manifestation of a more cooperative aspect of the dynamics, analogous to that of the viscosity in fragile fluids. The use of the VTF equation to describe the behavior of the conductivity in Li_2SO_4 has already been suggested in reference 16. In the strong-fragile classification, all the superionics shown are fragile and, of the two superionics simulated by us, lead fluoride is more fragile than calcium fluoride.

The temperatures in the upper part of Figure 1 have been scaled by the temperature at which the conductivity has fallen to $\sim 10^{-2.2}\ \Omega^{-1}\ cm^{-1}$. In the lower part, the temperature at which the viscosity reaches 10^{13} poise, i.e., the experimental glass transition temperature, is used. [We use the scaling temperature T_0 for the superionic data because it is something like the definition of the experimental glass transition temperature. For simulated CaF_2 and PbF_2, the values of T_0 are 810 and 1175 K, respectively. The appearance of the plot changes little with other choices of scaling temperature, for instance we could have used T_c, the location of the heat-capacity peak, but instead we introduce and discuss more thoroughly that feature below.]

Below this temperature all of the conductivities exhibit a simple Arrhenius temperature dependence, and we assume that in this region that the conductivity is due to independently hopping defects, or at least that the "cooperative" effects we wish to study have largely disappeared. Although the plots for the viscosity of the fragile liquids and the conductivities of the superionic systems are similar in shape, we note that the noticeably non-Arrhenius region covers approximately 3 orders of magnitude in the superionic case but nearly 10 orders for the supercooled liquids.

It seems plausible to associate the fragile aspects of the dynamics in the superionics to a cooperativity in the structure or motion of defects. A tendency for the defects to cluster has already been noted in diffuse neutron scattering experiments on PbF_2[3] and seen in simulations.[4,5] Also, the low temperature state of a superionic is the well-understood crystal, not the intractable glass. We hope not only to understand superionics better, and the origin of their similarities to supercooled liquids, but also to learn something more general about properties that the two classes of material have in common.

Both the conductivity and the viscosity are measures of collective (as opposed to single-particle) motion. If defects in the crystal are present in small quantities and their motion independent, the Nernst−Einstein equation relates the conductivity to the self-diffusion constant,

$$\sigma_{NE} = \beta\rho D \tag{1}$$

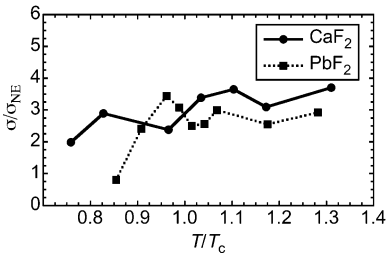

Figure 2. Ratio of the conductivity to the Nernst−Einstein conductivity for calcium fluoride and lead fluoride. At higher temperatures the ratio seems roughly constant, as is suggested by the similar Adam−Gibbs parameters for diffusivity and conductivity. The results for our lower temperature runs are omitted because the conductivity is not known with sufficent accuracy. The values included here are accurate within a range of approximately ± 0.5, so that we can be confident that the ratio is around 3 and slowly increasing through the transition. The oscillations in the curve are not reliable.

where $1/k_B\beta$ is the temperature with k_B Boltzmann's constant, ρ is the number density of mobile ions and D their self-diffusion coefficient. If the defects have a tendency to move together the true conductivity will be higher than the Nernst−Einstein conductivity, and if their motions tend to cancel it will be lower. The ratio of the conductivity to the Nernst−Einstein conductivity is shown in Figure 2 for both simulated superionics. The ratio (Haven's ratio) is greater than one, and increasing through the transition so that the conductivity is greater than can be explained by the independent motion of defects. This ratio is a second indicator of cooperativity in the defect dynamics, along with the fragile nature of the temperature dependence of the conductivity. The ratio shows that the defects do not move independently, but, since the ratio is only weakly temperature dependent, this dynamical correlation does not account for the strong temperature dependence of the conductivity, which must also be present in the single-particle motion.

We now have two measures of deviation from the simple dynamics of independent defects, for which the self-diffusion coefficient and the conductivity should be Arrhenius. The Haven's ratio value is evidence of "cooperativity", as the ions must move in a correlated way in order to account for the fact that it is substantially greater than unity, and increasing through the superionic state. The other measure is the fragility, or deviation from the Arrhenius Law. Haven's ratio compares conductivity to self-diffusion coefficient, *both* of which are non-Arrhenius. The usual interpretation for the fragility in a supercooled liquid is that the relaxation becomes more and more "cooperative" on cooling, in that larger and larger regions must relax as one to release the stress, and the activation energy for such an event increases with the size of the region involved. It is with the explanation for the fragility aspect of cooperativity in a superionic system with which we are primarily concerned in this work.

3.2. Two-Step Relaxation in Time-Correlation Functions. Supercooled liquids exhibit two-step relaxation in their time-correlation functions and also nonexponential relaxation ("stretching") at long times. For comparison we consider the self-intermediate scattering function of the fluoride ions in the superionic systems,

$$F_S(\mathbf{k},\tau) = \langle \exp(i\mathbf{k}\cdot(\mathbf{r}(\tau) - \mathbf{r}(0))) \rangle \tag{2}$$

where $\mathbf{r}(\tau)$ is the position of any anion at time τ, and the average makes this correlation function independent of the choice of anion. If a particle is taken initially at the origin, $F_S(\mathbf{k},\tau)$ describes the average decay in time τ of a Fourier component

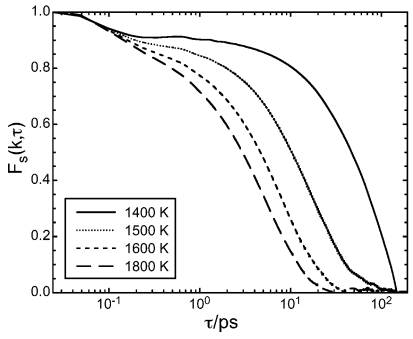

Figure 3. Self-intermediate scattering function ($F_S(\mathbf{k},\tau)$) for calcium fluoride, at $\mathbf{k} = (1/3, 1/3, 0)2\pi/a$, where a is the size of the cubic fluorite unit cell, and several temperatures. The self-decay shows two-step relaxation. The short-time decay describes the dephasing of vibrations, the second the slow escape of an ion from its site. This type of relaxation is typical of glass formers also, where the slow step might be regarded as the escape of a particle from the cage of its neighbors, but the similarity is a little superficial since this type of relaxation is almost forced by the superionics' crystalline matrices.

with wavevector **k** of the particle's probability distribution. Figure 3 shows the self-intermediate scattering function of fluoride ions in simulated calcium fluoride. The function is calculated for a wavevector that is considerable smaller than the inverse lattice constant; i.e., the function will only relax completely on a time scale at which a typical particle has moved from one unit cell to another. At low-temperature two-step relaxation is marked; an incipient plateau appears at the highest temperature. The long-time decay exhibits a strong temperature dependence.

At short times, before the appearance of a defect at the particle's site, the self-intermediate scattering function decays to a plateau value because of the dephasing of normal lattice vibrations. After the appearance of a defect, the particle may move over appreciable distances, completing the relaxation of the function. One of the predictions of the mode-coupling theory of the glass transition is that the initial decay of the slower relaxation step has the same functional form at all temperatures, but that the relaxation time varies with temperature.[17] Since the long-time decays on the self-intermediate scattering function are exponential, with a Kohlrausch−Williams−Watts parameter of 1.00 ± 0.03, this "time−temperature superposition" is trivially satisfied for the superionics. The observation of two-step relaxation in the single-particle motion is therefore a rather superficial point of similarity between the superionics and supercooled liquids.

3.3. Heat Capacity and Compressibility. The isobaric heat capacities of some fluorite-structured superionics are shown in Figure 4. They show a peak (whose position is normally taken to identify the transition temperature) that rises from a background of roughly $3k_B$ per ion, the equipartition value for a harmonic crystal. The height of the peak varies strongly from one material to another, with a more pronounced peak for the more "fragile" PbF_2 system compared to CaF_2. Supercooled liquids also exhibit a heat capacity peak (or, at least, a step) close to the glass transition, and its strength increases with the degree of fragility of the fluid.[6,15,18] However, we must be careful in drawing this analogy, since in the superionic we mean the true thermodynamic heat-capacity, whereas the supercooled liquid is in the process of falling out of equilibrium. In the supercooled liquid, the strength of the observed peak and the temperature at which it occurs depend on the rate of cooling and also, to some extent, the thermal history of the system. That is, the normally observed heat capacity feature is strongly

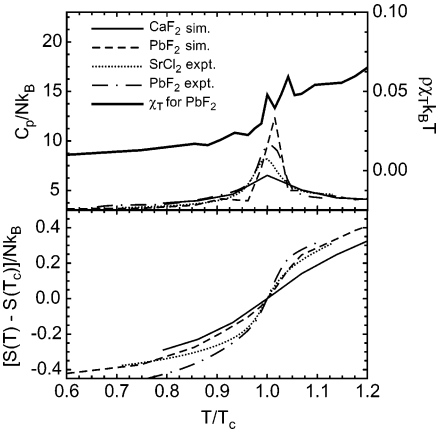

Figure 4. (upper frame) Isobaric heat capacities per ion calculated from simulation for CaF_2 and PbF_2, along with experimental values for lead fluoride[2] and strontium chloride[3]; along with the simulated isothermal compressibility. T_c is the temperature at which the heat capacity peak occurs. The simulated heat capacities come from the internal energy calculated from the simulations. (lower frame) Entropies calculated from the heat capacities using equation 3. The larger entropy changes near the transition correspond to sharper conductivity variation, i.e., to more fragile superionics.

affected by the fact that the supercooled liquid is undergoing a transition to a nonequilibrium state. Nevertheless, computer simulations of a simple model glass former[19] have confirmed that there is an underlying heat capacity peak in a model supercooled liquid (which would be anticipated from the energy landscape picture[6]) and that it is independent of the preparation of the configurations. The superionic systems show a heat capacity *peak*, rather than the shoulder that is more characteristic of a supercooled liquid, because the crystalline matrix in the superionic imposes a limit on the amount of disorder, and the rate of increase in the number of available microstates saturates.

Figure 4 also shows a peak in the isothermal compressibility, from the simulations for lead fluoride, at the superionic transition. We note that the change in the compressibility occurs at the same temperature as the heat capacity peak. Again, changes in the elastic moduli at the glass transition have been reported from light and X-ray scattering measurements on supercooled liquids.[20] The compressibility plays an important role in some models for the cooperativity at the superionic transition. If the creation of one defect softens the lattice and increases its compressibility, a second may be more easily created. This softening has been used as the basis of a mean-field model of the superionic transition.[21,22]

3.4. Entropy and the Adam−Gibbs Relationship. The entropy per ion calculated from the heat capacity is also shown in Figure 4,

$$\frac{\Delta_{12}S}{Nk_B} = \int_{T_1}^{T_2} \mathrm{d}T \left[\frac{C_p}{Nk_B T} - \frac{3}{T}\right] \qquad (3)$$

where N is the number of ions, k_B is Boltzmann's constant, T the temperature, C_p is the isobaric heat capacity per ion from the upper pane of Figure 4, and $\Delta_{12}S$ is the change in entropy between T_1 and T_2, apart from the divergent, harmonic part proportional to log T. In Figure 4, T_1 is taken to be T_c, the location of the heat-capacity peak. We will discuss the relationship between the total entropy and the entropy associated with the creation of defects in the lattice below, but first we note a connection between the entropy and the ion dynamics, which is similar to that frequently observed in glass-forming systems.

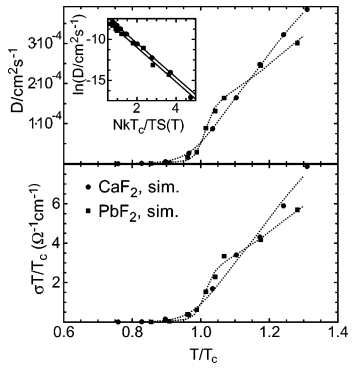

Figure 5. Fits of self-diffusion constants to the Adam−Gibbs equation along with similar fits for $\sigma T/T_c$, the conductivity multiplied by the scaled temperature. Note that the lead compound is more fragile, as judged by either transport coefficient, and that the Adam−Gibbs equation describes both transport coefficients equally well.

TABLE 3: Parameters Obtained by Fitting to the Adam−Gibbs Equation[a]

	A	C
D/cm^2 s^{-1} (PbF_2)	$(1.1 \pm 0.2) \times 10^{-3}$	2.1 ± 0.2
D/cm^2 s^{-1} (CaF_2)	$(1.9 \pm 0.1) \times 10^{-3}$	2.1 ± 0.06
$(\sigma T/T_c)/\Omega^{-1}$ cm^{-1} (PbF_2)	20.9 ± 4.2	2.1 ± 0.28
$(\sigma T/T_c)/\Omega^{-1}$ cm^{-1} (CaF_2)	40.7 ± 10.0	2.25 ± 0.30

[a] Fitting log D against $(TS)^{-1}$ using linear least squares gives parameter values very similar to the results of Levenberg−Marquardt nonlinear least-squares fitting of D as a function of TS_c.

The Adam−Gibbs equation relates the self-diffusion constant, D, to the configurational entropy:[23,24]

$$D = A \exp\left(-\frac{\beta C}{S_c}\right) \tag{4}$$

where C is a constant, A is the high-temperature limit of the diffusion constant, and S_c is the configurational entropy. In a modern interpretation,[25,26] the configurational entropy describes the number of available basins on the potential-energy landscape, and the Adam−Gibbs relation suggests a link between the number of basins and the mobility.

Figure 5 shows a fit of the Adam−Gibbs equation to our simulated fluoride self-diffusion constants, using the entropy from thermodynamic integration (equation 3), *not* the true configurational entropy. However, as we will see below, the variation of this entropy near the transition is largely configurational, so its substitution for S_c seems reasonable. We also note that a rough proportionality of excess and configurational entropies holds for some glass formers, so the Adam−Gibbs equation works reasonably well for both.[25] The two parameters A and C were varied in the fit, and are given in Table 3. Figure 5 and Table 3 also include Adam−Gibbs fits to the reduced conductivity $\sigma T/T_c$, as a function of scaled temperature. The qualities of both sets of fits are similar, so the Adam−Gibbs equation describes conductivity just as well as self-diffusion, which is convenient because more experimental data is available for the conductivity than the diffusion coefficient.

Figure 6 shows an Adam−Gibbs plot of experimental conductivity data on strontium chloride,[3,8] i.e., $\log(\sigma T)$ against $k_B T_c/(TS(T))$, where S is the entropy from equation 3. In the same figure we contrast the Adam−Gibbs fit with an Arrhenius plot of the same conductivity data. The two curves are close at low temperatures, where the entropy varies slowly and conductivity is simply activated. At *very* low temperatures ($T_c/T > 1.25$) the extrinsic defects (due to impurities and grain

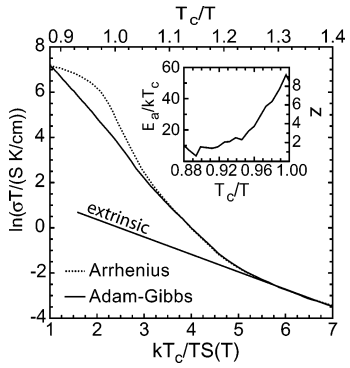

Figure 6. Adam−Gibbs plot of experimental conductivity data for strontium chloride (solid curve using the bottom axis) and the Arrhenius plot of the same data for comparison (dotted curve and upper axis). The two curves agree except in the superionic region, where the entropy is changing rapidly. The inset shows the effective activation energy (i.e., the slope of the Arrhenius curve in the main plot), which is of very little use itself, but since the Adam−Gibbs equation works well we may estimate the extent of cooperativity from it. The right-hand axis of the inset gives the value of this parameter z, which might be the size of a group of relaxational units that move cooperatively. This is related to the usual interpretation of the Adam−Gibbs equation, for which see reference 4.

boundaries in the experimental material) take over from the intrinsic, thermally generated ones, and so the activation energy changes, according to Voronin and Volkov, who performed the conductivity measurements.[8] See also the discussion of different contributions to the conductivity of ionic crystals in reference 1.

Consider now the region at higher temperatures, between $T_c/T = 0.9$ and 1.2. As the superionic transition is approached on heating, the Arrhenius curve (dotted) begins to deviate from linearity, showing the effect we have associated with "fragility", but the Adam−Gibbs curve (solid) continues with nearly the same slope. Figure 6 shows that the Adam−Gibbs equation agrees with the experimental data far better than the Arrhenius law, and this for one of the most fragile superionics. Even if the change of slope at around $T_c/T \approx 1.025$ is regarded as a flaw, the Adam−Gibbs equation does hold well for a variation in conductivity of more than an order of magnitude, and this variation is in the most non-Arrhenius regime. We note also that, if strontium chloride behaves like the other fluorite-structured superionics, the lattice expands quite sharply around T_c. The Adam−Gibbs equation therefore appears to recover some of the simplicity of the Arrhenius law for complex, cooperative dynamics.

It has been argued that the Adam−Gibbs relationship is not a fundamental aspect of the glass transition in supercooled liquids. From the energy landscape perspective, the configurational entropy corresponds to the number of accessible energy minima or basins, but dynamics should depend on the heights of barriers between these basins. If the barriers between the basins were raised, without modifying the number or shape of the basins, the dynamics would slow, but the configurational entropy would not change.[27] This argument implies that the Adam−Gibbs equation cannot hold in general, but does not mean that it cannot hold for some class of materials. It may be that for such a class the barriers do not vary independently of the basins. It is somewhat easier to argue for a connection between entropy and dynamics for the ionic conductors since ions can only move in the presence of defects and, as we will now show, these defects make a large contribution to the increase in entropy of the ionic conductors in the vicinity of the superionic transition. We note that a similar argument

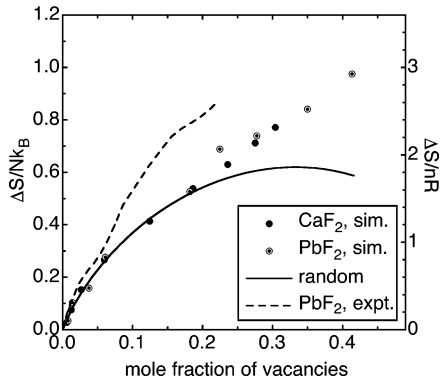

Figure 7. Entropies shown in Figure 4 now plotted against the fraction of anions that are off their perfect-crystal sites. The curves are all shifted to agree at zero defect concentration. The left axis has the entropy per ion, the right has entropy per mole of PbF_2. The simulated calcium and lead fluoride defect data come from counting the number of empty tetrahedra of lead ions. The experimental lead fluoride curve is taken from the fit shown in reference 2 to the results of scattering experiments. This curve agrees with the simulation results reasonably well, given that the experimental defects are not the same as those found in a simulation. It is remarkable that all three curves are so close.

supports the Adam−Gibbs relation when applied to a Fredrickson−Anderson kinetic Ising model, for which it holds over 6 orders of magnitude.[28,29]

4. Defects, Entropy, and Dynamics

In reference 5 we produced a measure of the number of defects present in an instantaneous ionic configuration from the computer simulations by exploiting the geometry of the fluorite lattice. In the ideal lattice, the fluoride ions occupy the tetrahedral sites in the cubically close-packed cation lattice. At a finite temperature, we can identify vacancies (equal to the number of vacancy-interstitial pairs) by counting the number of empty tetrahedra, formed from the *instantaneous* positions of any four neighboring cations. In PbF_2 we showed that this vacancy count and its temperature dependence agreed well with that obtained directly from diffraction data by Goff et al.[2] The number of defects rises rapidly in the vicinity of transition and then approaches a plateau at which one-quarter to one-third of the fluoride ions are off their lattice sites. In the remainder of the paper we will examine whether we can relate this "observable" number of defects to the thermodynamic and dynamic properties.

Figure 7 shows the entropies from Figure 4 as a function of the number of defects, for the simulation models of CaF_2 and PbF_2 and from experimental data for PbF_2.[2] All entropy curves in Figure 4 have been shifted to agree where the defect concentration vanishes. Though the interaction potentials and the temperature dependence of the heat capacity of the two materials are very different, the variations of entropy with defect population are very similar. The experimental curve is taken from the experimental heat capacity and a fit to vacancy concentration data in reference 2. The experimental curve is quite close to the simulated ones; given that the defects obtained from the diffraction measurements are not the same as our geometrically defined ones, we consider this to be good agreement. We will examine the relationship between the number of defects and the entropy more closely below.

The sharp increase in the number of defects at the transition must be linked to the non-Arrhenius behavior of the mobility, since in a crystalline lattice all ionic hopping processes occur via the creation and destruction of defects. However, this link

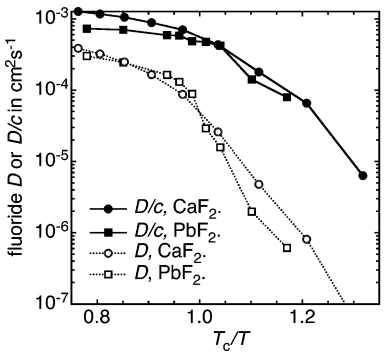

Figure 8. Diffusion constants for fluoride ions in the two simulated superionics and the same quantity divided by the concentration of defects, both plotted against scaled inverse temperature, in the manner of an Angell plot. Dividing by the concentration of defects is not enough to remove the fragile temperature dependence of the diffusion coefficient, but note that D/c varies over fewer decades.

is not the simple one that would be expected on an independent defect model, where the mean ionic diffusion coefficient is proportional to the number of defects multiplied by a kinetic coefficient that reflects the migration rate of a defect. To emphasize this point we show in Figure 8 an Arrhenius plot of the mean ionic diffusion coefficient *divided by the number of defects* versus (scaled) inverse temperature. In the simple model, we would expect such a plot to be near-linear, with a slope reflecting the activation energy of the defect migration. In fact, we see that the plot deviates from Arrhenius almost as strongly as the diffusion coefficient itself. This shows that the dependence of the diffusion coefficient on the number of defects in the vicinity of the transition is much stronger than Arrhenius. The fragile, non-Arrhenius temperature dependence observed in the diffusion coefficient is not, therefore, simply due to the rapid increase in the number of defects. There is a cooperative aspect in the kinetics of the process that seems to reflect the participation of more than one defect in the ionic hopping events in the vicinity of the transition. This is reminiscent of the scenario represented by kinetic Ising models of the glass transition,[28,30,31] where the rate at which a defect is created or destroyed on a lattice site depends on the number of defects on neighboring sites.

4.1. Defects and the Collective Dynamics. As we remarked above, time correlation functions in the superionic systems show two-step relaxation, but single-particle correlation functions, such as the self-intermediate scattering function, show relaxation characteristics different than the collective ones. We define the Fourier components of the instantaneous densities as

$$\rho_\alpha(\mathbf{k}, t) = \sum_{j=1}^{N_\alpha(t)} \exp(i\mathbf{k}\cdot\mathbf{r}_{j\alpha}(t)) \qquad (5)$$

where α denotes either interstitials, vacancies, or fluoride ions on their perfect-crystal sites; $\mathbf{r}_{j\alpha}(t)$ is the position of the jth particle of species α at time t; and $N_\alpha(t)$ is the number of particles of species α at time t. The fluoride ions have been divided into on-site ions and interstitials at each time, according to whether the ions are within or outside one of the tetrahedral sites within the Pb^{2+} lattice, as described above. The positions of the vacancies appearing in eq 6 are the centers of the empty tetrahedra. Here we consider the time correlation function of these density fields, $F_\alpha(\mathbf{k},\tau)$,

$$F_\alpha(\mathbf{k},\tau) = \langle \rho_\alpha(\mathbf{k}, t)\rho_\alpha(-\mathbf{k}, 0)\rangle \qquad (6)$$

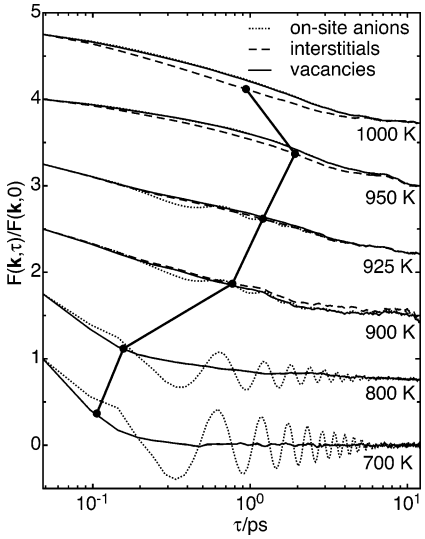

Figure 9. Decay of fluctuations ($F(\mathbf{k},\tau)/F(\mathbf{k},0)$), at $\mathbf{k} = (1/3, 0, 0)2\pi/a$, where a is the size of the cubic fluorite unit cell, in the density of on-site anions, of interstitials and of vacancies for lead fluoride. The vacancy positions are the centers of unoccupied tetrahedra of lead ions. Oscillations in the on-site anion density disappear above the superionic transition as the fluorides begin to flow freely and independently. The thick black line joins the points at which the interstitial function has decayed to $1/e$. This relaxation time becomes short at low temperatures, as defects cease to be a long-lived species.

which measures the relaxation of collective density fluctuations of the species α (see reference 32 for examples of similar correlation functions). In Figure 9, normalized functions $F_\alpha(\mathbf{k},\tau)$ calculated for different subsets of ions and defects (i.e., different α in eq 6) are shown for PbF_2 over a range of temperatures which span the superionic transition. The calculations have been made for the wavevector $(1/3, 0, 0)2\pi/a$, where a is the size of the cubic unit cell. Our simulation cell is a $3 \times 3 \times 3$ cube of cubic fluorite unit cells. This wavevector corresponds approximately to the distance between neighboring octahedral sites. The functions have all been normalized by dividing them by their values at $\tau = 0$.

Well below the superionic transition (700 K and 800 K), there are few defects in the system. The total fluoride correlation function is dominated by the on-site anions and shows the typical behavior of a high-temperature solid—a damped oscillatory decay at the frequency of a longitudinal phonon of the crystal. At these low temperatures the correlation functions for the defects (vacancies and interstitials) agree closely. Both decay rapidly, reflecting the very rapid recombination of vacancies and interstitials, inside one vibrational period of the on-site function. The damping of the phonons becomes pronounced on approaching the superionic transition, so that even by 900 K (which is still below the transition at ~940 K in the simulated system) the oscillatory character of the on-site ion correlation function is lost and the function relaxes in a diffusional, high-k liquid-like manner. In this region all three correlation functions relax similarly. The thick black line joins the points at which the interstitial function has decayed to $1/e$. This relaxation time becomes short at low temperatures, due to the rapid vacancy—interstitial recombination. This recombination rate slows as the temperature increases toward the transition. Above the transition (950 K and 1000 K), the relaxation time is now decreasing with T and the decay looks more like that of a supercooled liquid. In this regime, the growth in defect number with temperature slows, but the defects, and so the ions, flow more freely. At 950 K the relaxation even has two steps, though they are not well separated. These decays show a crossover from the rapid annihilation of isolated vibrational defects at low temperatures to the collective decay of the density of the many defects above the transition. The low-temperature crystal has a small conductivity due to the occasional hopping of a few defects, but above T_c the disorder and mobility are both much greater, and the relaxation more like that of a liquid. This is reminiscent of the crossover from "hopping processes" below the ideal glass transition to collective processes above it (but note that the hopping processes in a glass are very much slower).[17]

5. Modeling the Defect Concentration

We have seen that the rapid, nontrivial temperature dependences of the mobility and entropy in the superionic systems close to the transition temperature may both be linked to a rapid increase in the number of "defects" (as defined above, in terms of the occupation of tetrahedral sites in the Pb^{2+} lattice). This observation provides a rationale for a connection between the entropy and mobility which we have seen is given by a relationship of Adam—Gibbs form. It suggests an analysis of the temperature dependence of the defect concentration as a first step to account for the "fragile", non-Arrhenius temperature dependence of the mobility and for the origin of the "cooperativity" which it is believed to reflect.

We now turn to the origin of the rapid increase in the concentration of defects. It indicates that the free energy of defect formation is lowered as the defect concentration is increased through some critical range. This could be due to a number of factors, which we hope to differentiate in the remainder of this and the following paper.[37] It has been suggested that defect formation increases the vibrational entropy of the lattice and also lowers the elastic constants, thereby reducing the strain energy associated with defect formation.[6,33] In experiments and simulation there is evidence of a favorable interaction between defects, since they are observed to cluster.[3,5]

A starting point is to examine how the observed entropy is related to the configurational entropy calculated by randomly placing the defects on the possible sites. If we remove n randomly chosen fluoride ions from the M ions available on the perfect lattice, and place them randomly on the αM available interstitial sites, we find the configurational entropy to be

$$\frac{S_r}{k_B} = \log\left(\frac{M!}{n!(M-n)!}\right) + \log\left(\frac{(\alpha M)!}{n!(\alpha M - n)!}\right) \qquad (7)$$

The subscript 'r' refers to the random placement. We find in the simulations that only one interstitial at a time may fit into a given octahedron, so that α is one-half. With few defects (below the transition temperature, where the heat capacity peak is observed), the entropy from the thermodynamic integration is similar to this random value (see again Figure 4). The observed entropies then grow more quickly above the transition than can be accounted for by randomly arranged defects. If the defects are interacting, they should be ordered somehow and the observed entropy should be lower than the random configurational entropy, but instead it is higher. This points to other factors affecting the thermodynamics of defect formation in the transition region.

5.1. Mean-Field Models. Mean-field theories write the free energy in terms of the concentration of defects on a lattice, it does not depend on their distribution in space. The important element is the representation of the interaction between the defects as an excess chemical potential. The usual form for this

potential is a power law,

$$\mu_{ex} = -Jc^m \tag{8}$$

where J is a coupling constant, c the fraction of vacant tetrahedra, and m is a constant power, usually less than unity. A drawback of the method is that we do not know the interaction in detail. In fact, the same excess potential for use on superionics has been derived from several different physical pictures.[1,34]

Information about the lattice geometry enters the model through the configurational entropy. This is the same as the quantity in equation 7, but with the use of Stirling's approximation it takes the form

$$s_r = \alpha \log \alpha - 2c \log c - (1-c)\log(1-c) - (\alpha - c)\log(\alpha - c) \tag{9}$$

where c is the fraction of anions that have left their lattice sites and α the maximum possible value for c. This equation is equivalent to eq 7, but in a form more appropriate to a mean-field model. The term s_r is defined here as the entropy per fluoride ion in units of k_B, as the cations are not included in mean-field models. The final ingredient is the free energy of creation of an isolated defect, $h - Ts$. We regard h as the enthalpy required to move an anion into an interstitial site and s to include the change in vibrational entropy due to any change induced in the vibrational modes by the presence of a defect.

The free energy is then written

$$\beta g = c(\beta h - s) - s_r + \beta g_{ex}(c) \tag{10}$$

$$g_{ex}(c) = \int_0^c dx\, \mu_{ex}(x) \tag{11}$$

The free energy is implicitly regarded as a Gibbs free energy, as we are interested in the experimentally familiar case of constant pressure. Note, however, that there is no explicit mention of the density: in using the concentration as the independent variable, we subsume variations in the unit cell volume into the defect creation enthalpy and the excess chemical potential. By minimizing the free energy, a prediction for the number of defects as a function of temperature is obtained.

Having chosen a value for m, on the basis of a particular model for the defect interactions, the theory will have three parameters: the defect creation enthalpy, h, and entropy, s, and the coupling parameter J. The most common choice is $m = 1$,[1] sometimes called the "two-state model". This has been proposed to describe the behavior of viscous liquids,[7] particularly the tetrahedral network fluids mentioned in section 1. If the defects have Coulombic interactions screened by other defects, the Debye−Hückel interaction is the result, which leads to $m = 1/2$. Maier et al. have proposed using $m = 1/3$ to represent a screened Coulombic interaction, which also allows for a dielectric screening by the polarizabilities of the fixed ions, in analyzing several superionics.[35,36] Note that though we follow the common practice of calling the $m = 1$ model the "two-state model", all models describe a lattice of sites that may be in either of two states. The models described above appeal to electrostatics to explain the interactions of defects, but there is an alternative. Defects soften the lattice, and this may favor the creation of more defects. Rice, Strässler and Toombs argued for this explanation and used it to derive the two-state model ($m = 1$).[21] A similar picture is used by Granato in analyzing defect contributions to the free energy of face-centered-cubic metals.[33] The large diaelastic softening of shear modulus on creation of one defect lowers the creation energy for another. Granato's model also incorporates the effect of defect creation on the vibrational entropy. The noticeable increase in isothermal compressibility at the superionic transition and above (Figure 4) supports a role for lattice softening in defect interactions. We return to this possibility in the following paper.[37]

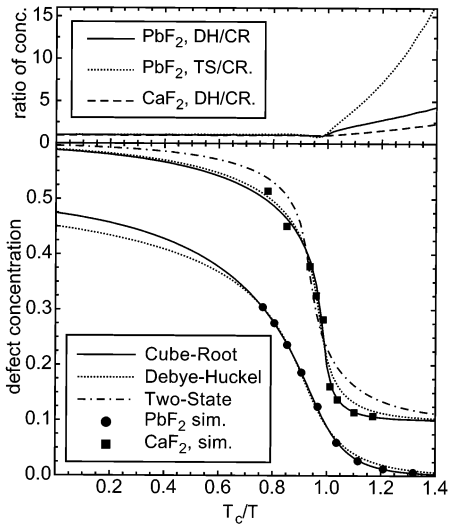

Figure 10. (lower plot) Fits of the simulated defect population data for lead fluoride and calcium fluoride to the cube-root and Debye−Hückel mean-field models. The cube-root model is clearly superior. The two-state model ($m = 1$) is shown for PbF_2 only and is still worse than the Debye−Hückel model. (upper plot) Ratios of the Debye−Hückel and two-state solutions to the better cube-root model, emphasizing that they fail badly below the transition.

TABLE 4: Parameters Obtained by Fitting the Debye−Hückel (DH), Cube-Root (CR), and Two-State (TS) Models to Simulated Defect Populations[a]

substance	model	h/k_BT_c	s/k_B	J/h
PbF_2	CR	13.7	3.7	1.0
PbF_2	DH	11.1	3.8	1.1
PbF_2	TS	9.4	4.9	1.3
CaF_2	CR	11.4	2.5	1.0
CaF_2	DH	9.1	2.0	1.2

[a] The curves obtained from these parameters are shown in Figure 10. The transition temperatures are 936 K for lead fluoride,[5] and 1450 K for calcium fluoride.

Figure 10 shows fits of Maier's cube-root model and the Debye−Hückel model to our data on the concentration of defects for both simulated superionics, and a fit of the two-state model to the lead fluoride data. The parameters from the fits are given in Table 4. The cube-root model clearly provides a better fit than the other two. Its sharper variation in the excess chemical potential at low concentration is necessary to produce a point of inflection in the temperature dependence of the defect concentration at low concentrations, as noted in reference 36. The other models cannot reproduce both high and low temperature data. The upper panel of Figure 10 shows that the Debye−Hückel and two-state models particularly fail below the transition. It would no doubt be possible to find Debye−Hückel parameters that fit well below the transition, but the same parameters would not work well above.

The values for the enthalpy of formation of a single defect obtained by fitting the cube root model are, at 1.1 eV and 1.4 eV for PbF_2 and CaF_2, respectively, reasonable values for this quantity in the high-temperature range where the fit is applied.[1] The lead fluoride and calcium fluoride coupling coefficients (J) are similar in units of k_BT_c. The actual coupling is then larger

for calcium fluoride, though, as we have seen, the lead compound is more fragile. The parameter that is noticeably different for the two is the entropy s, which is larger for PbF_2. It is the entropy contribution s that determines the drive to higher energy, more mobile states, and so determines the fragility. This is similar to the situation proposed for glass formers.[6,7]

It would seem, therefore, that the cube-root model can provide a good representation of the temperature dependence of the defect concentration, with physically sensible values for the various interaction parameters. The model should be thermodynamically consistent and allow the thermodynamic properties to be predicted with the same parameters. The entropies calculated from the cube-root model, $sc + s_r(c)$, are significantly larger (about 50%) than those from thermodynamic integration and from randomly distributing the defects. The problem is due to the term in the defect creation entropy, sc, which overestimates the entropy of creation of an isolated defect. This term was vital to account for the rapid increase in defect number with temperature which, in turn, we have linked to the degree of fragility. One of the more general mean-field treatments of superionics was given by Welch and Dienes.[22,34] They included a quadratic entropy dependence on concentration. Such an addition could hardly improve the cube-root fits to defect concentration in Figure 10, but it might help to reproduce the entropies shown in Figure 4.

6. Summary and Discussion

We have described several phenomenological similarities between the glass transition in fragile supercooled liquids and the superionic transition in "type-II", fluorite-structured materials. Notable among these is the success of the Adam−Gibbs relation in connecting the non-Arrhenius temperature dependence of the diffusivity and conductivity of the superionics in the transition regime nonharmonic entropy. The Adam−Gibbs relation holds over most of the superionic regime, where the departure from Arrhenius behavior is the greatest, and this for the most fragile superionic we examine, strontium chloride. A plausible reason for this relationship, in the superionic case, is that both the entropy and the ion dynamics can be expected to be related to the number of defects present in the system at each temperature.

The entropy shows the same smooth dependence on defect number for both simulated systems, despite their different thermal properties, interaction potentials, etc. The number of defects is defined as the number of fluoride ions not within the tetrahedral sites of the cation lattice. This definition is supported by diffraction studies on PbF_2, from which a number of off-site fluoride ions can be measured[2] and found to behave very similarly to the simulation quantity. The superionic system, in which the concept of a defect is readily realized in a concrete form, therefore appears to exhibit many of the characteristics proposed in bond-defect models of the glass transition.

A reasonable first step in producing a theory of the cooperative aspects of the superionic transition would therefore seem to be to produce a theory for the temperature dependence of the number of defects that correctly reproduces the energy and entropy variation with temperature. This would be followed by a dynamical theory to understand how the transport coefficients depend on the defect number. However, even the first step does not seem to be straightforward. A cube-root mean-field model, as proposed by Hainovsky and Maier,[36] fits the form of the temperature dependence of the defect concentration quite well (considerably better than other mean-field theories), and the parameters extracted from the fit give reasonable values for the enthalpy and entropy of formation of a single defect. However, with the same parameters, the theory does not predict the entropy at all well.

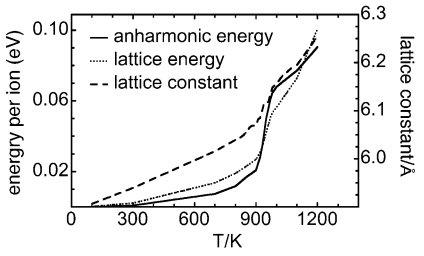

Figure 11. Anharmonic internal energy and lattice energy of lead fluoride in the vicinity of the transition. The lattice energy is the energy of the perfect crystal at the appropriate density, with lattice constant the same as that used for the simulations. The lattice constant is also shown.

Another manifestation of the inconsistency of the thermodynamics with the defect picture is seen when we examine the enthalpy change across the transition. Figure 11 shows the lattice energy and anharmonic energy across the transition for lead fluoride. The lattice energy is obtained from the energy of a perfect fluorite lattice (at 0 K) at the density appropriate to the finite temperature, zero-pressure simulations: we have seen that this density changes quite sharply through the transition (see also ref 2 for experimental information). The anharmonic energy is obtained from the total internal energy of the simulation by subtracting the equipartition harmonic value of $3k_BT$ per particle. Since our simulations were carried out at zero pressure, the internal energy and the enthalpy are the same. We might expect the anharmonic energy to reflect the energy cost of creating a number of (interacting) defects together with any consequential increase in the degree of anharmonicity due to a change in the character of the vibrational modes in the defective lattice. However, the data in the Figure 11 suggest an alternative viewpoint: the change in the perfect crystal lattice energy accounts for a substantial share of the increase in anharmonic energy across the transition (though the two curves do not quite follow each other). The realization that the thermodynamic consequences of the lattice expansion are substantial may also help to explain why above the transition the entropy is greater than that obtained by randomly placing the defects (see Figure 7).

We take up the problem of how to relate the degree of disorder of the crystal to its thermodynamic properties in the following paper.[37]

References and Notes

(1) Chandra, S. *Superionic Solids: Principles and Applications*, North-Holland: Amsterdam, 1981.

(2) Goff, J. P.; Hayes, W.; Hull, S.; Hutchings, M. T. *J. Phys.: Condens. Matter* **1991**, *3*, 3677.

(3) Hutchings, M. T.; Clausen, K.; Hayes, W.; Kjems, J. K.; Schnabel, P. G.; Smith, C. *J. Phys. C: Solid State Phys.* **1984**, *17*, 3903.

(4) Castiglione, M. J.; Wilson, M.; Madden, P. A.; Grey, C. P. *J. Phys.: Condens. Matter* **2001**, *13*, 51.

(5) Castiglione, M. J.; Madden, P. A. *J. Phys.: Condens. Matter* **2001**, *13*, 9963.

(6) Moynihan, C. T.; Angell, C. A. *J. Non-Cryst. Solids* **2000**, *274*, 131.

(7) Angell, C. A.; Moynihan, C. T. *Metall. Mater. Trans. B* **2000**, *31B*, 587.

(8) Voronin, B. M.; Volkov, S. V. *J. Phys. Chem. Solids* **2001**, *62*, 1349.

(9) Trnovcová, V.; Fedorov, P. P.; Smatko, I. I. B. V.; Hanic, F. *Solid State Ionics* **1999**, *119*, 181.

(10) Gillan, M. J. *J. Phys. C: Solid State Phys.* **1986**, *19*, 3391.

(11) Dent, A.; Wilson, M.; Madden, P. A. *Solid State Ionics* **2004**, *167*, 73.

(12) Rapaport, D. C. *The Art of Molecular Dynamics Simulation*; Cambridge University Press: Cambridge, 1997.

(13) Tuckerman, M. E.; Martyna, G. J. *J. Phys. Chem. B* **2000**, *104*, 159.

(14) Tuckerman, M. E.; Martyna, G. J. *J. Phys. Chem. B* **2001**, *105*, 7598.
(15) Angell, C. A. *Science* **1995**, *267*, 1924.
(16) Tärneberg, R.; Mellander, B.-E. *Solid State Ionics* **1997**, *98*, 175.
(17) Götze, W. Aspects of structural glass transitions. In *Liquids, freezing and glass transition*; Hansen, J.-P., Levesque, D., Zinn-Justin, J., Eds.; Les Houches, Session LI; Elsevier: Amsterdam, 1989; pp 287−503.
(18) Stillinger, F. H. *J. Phys. Chem. B* **1998**, *102*, 2807.
(19) Padilla, F. G.; Harrowell, P.; Fynewever, H. *J. Non-Cryst. Solids* **2002**, *307*, 436.
(20) Masciovecchio, C.; Monaco, G.; Ruocco, G.; Sette, F.; Cunsolo, A.; Krisch, M.; Mermet, A.; Soltwisch, M.; Verben, R. *Phys. Rev. Lett.* **1998**, *80*, 544.
(21) Rice, M. J.; Strässler, S.; Toombs, G. A. *Phys. Rev. Lett*. **1974**, *32*, 596.
(22) Welch, D. O.; Dienes, G. J. *J. Phys. Chem. Solids* **1977**, *38*, 311.
(23) La Nave, E.; Mossa, S.; Sciortino, F. *Phys. Rev. Lett.* **2002**, *88*, 225701.
(24) Adam, G.; Gibbs, J. H. *J. Chem. Phys*. 1965, *43*, 139.
(25) Angell, C. A.; Borick, S. *J. Non-Cryst. Solids* **2002**, *307*, 393.
(26) La Nave, E.; Mossa, S.; Sciortino, F. *Phys. Rev. Lett*. **2002**, *88*, 225701.
(27) Stillinger, F. H.; Debenedetti, P. G. *J. Chem. Phys*. **2002**, *116*, 3353.
(28) Fredrickson, G. H.; Andersen, H. C. *Phys. Rev. Lett*. **1984**, *53*, 1244.
(29) Fredrickson, G. H.; Brawer, S. A. *J. Chem. Phys*. **1986**, *84*, 3351.
(30) Kob, W.; Andersen, H. C. *Phys. Rev. E* 48, 4364 (193).
(31) Berthier, L.; Garrahan, J. P. *J. Chem. Phys*. **2003**, *119*, 4367.
(32) Förster, D. *Hydrodynamic Fluctuations, Broken Symmetry and Correlation Functions*; W. A. Benjamin: Reading, MA, 1975.
(33) Granato, A. V. *Phys. Rev. Lett*. **1992**, *68*, 974.
(34) Welch, D. O.; Dienes, G. J. *J. Electron. Mater*. **1975**, *4*, 973.
(35) Zimmer, F.; Ballone, P.; Parrinello, M.; Maier, J. *Solid State Ionics* **2000**, *127*, p277.
(36) Hainovsky, N.; Maier, J. *Phys. Rev. B* **1995**, *51*, 15789.
(37) Gray-Weale, A.; Madden, P. A. *J. Phys. Chem. B* **2004**, *108*, 6634.